Received 13 May 2004; accepted 10 January 2005; doi:10.1038/nature03356.


1. Nishimura, M. & Somerville, S. Plant biology. Resisting attack. *Science* **295,** 2032–2033 (2002).
2. Thordal-Christensen, H. Fresh insights into processes of nonhost resistance. *Curr. Opin. Plant Biol.* **6,** 351–357 (2003).
3. Bais, H. P., Fall, R. & Vivanco, J. M. Biocontrol of *Bacillus subtilis* against infection of *Arabidopsis* roots by *Pseudomonas syringae* is facilitated by biofilm formation and surfactin production. *Plant Physiol.* **134,** 307–319 (2004).
4. Yu, G. L., Katagiri, F. & Ausubel, F. M. *Arabidopsis* mutations at the *RPS2* locus result in loss of resistance to *Pseudomonas syringae* strains expressing the avirulence gene avrRpt2. *Mol. Plant Microbe Interact.* **6,** 434–443 (1993).
5. Davis, K. R., Schott, E. & Ausubel, F. M. Virulence of selected phytopathogenic pseudomonads in *Arabidopsis thaliana*. *Mol. Plant Microbe Interact.* **4,** 477–488 (1991).
6. Dong, X., Mindrinos, M., Davis, K. R. & Ausubel, F. M. Induction of *Arabidopsis* defense genes by virulent and avirulent *Pseudomonas syringae* strains and by a cloned avirulence gene. *Plant Cell* **3,** 61–72 (1991).
7. Debener, T., Lehnackers, H., Arnold, M. & Dangl, J. L. Identification and molecular mapping of a single *Arabidopsis thaliana* locus determining resistance to a phytopathogenic *Pseudomonas syringae* isolate. *Plant J.* **1,** 289–302 (1991).
8. Walker, T. S., Bais, H. P., Grotewold, E. & Vivanco, J. M. Root exudation and rhizosphere biology. *Plant Physiol.* **132,** 44–51 (2003).
9. Walker, T. S., Bais, H. P., Halligan, K. M., Stermitz, F. R. & Vivanco, J. M. Metabolic profiling of root exudates of *Arabidopsis thaliana*. *J. Agric. Food Chem.* **51,** 2548–2554 (2003).
10. Callaway, R. M. & Aschehoug, E. T. Invasive plants versus their new and old neighbors: a mechanism for exotic invasion. *Science* **290,** 521–523 (2000).
11. Bais, H. P., Vepachedu, R., Gilroy, S., Callaway, R. M. & Vivanco, J. M. Allelopathy and exotic plant invasion: from molecules and genes to species interactions. *Science* **301,** 1377–1380 (2003).
12. Nikaido, H. Multiple antibiotic resistance and efflux. *Curr. Opin. Microbiol.* **1,** 516–523 (1998).
13. Galan, J. E. & Collmer, A. Type III secretion machines: bacterial devices for protein delivery into host cells. *Science* **284,** 1322–1328 (1999).
14. Roine, E. *et al.* Hrp pilus: an *hrp*-dependent bacterial surface appendage produced by *Pseudomonas syringae* pv. *tomato* DC3000. *Proc. Natl Acad. Sci. USA* **94,** 3459–3464 (1997).
15. Xiao, Y., Heu, S., Yi, J., Lu, Y. & Hutcheson, S. W. Identification of a putative alternate sigma factor and characterization of a multicomponent regulatory cascade controlling the expression of *Pseudomonas syringae* pv. *syringae* Pss61 *hrp* and *hrmA* genes. *J. Bacteriol.* **176,** 1025–1036 (1994).
16. Zwiesler-Vollick, J. *et al.* Identification of novel *hrp*-regulated genes through functional genomic analysis of the *Pseudomonas syringae* pv. *tomato* DC3000 genome. *Mol. Microbiol.* **45,** 1207–1218 (2002).
17. Bender, C. L., Alarcon-Chaidez, F. & Gross, D. C. *Pseudomonas syringae* phytotoxins: mode of action, regulation, and biosynthesis by peptide and polyketide synthetases. *Microbiol. Mol. Biol. Rev.* **63,** 266–292 (1999).
18. Dixon, R. A. Natural products and plant disease resistance. *Nature* **411,** 843–847 (2001).
19. Papadopoulou, K., Melton, R. E., Leggett, M., Daniels, M. J. & Osbourn, A. E. Compromised disease resistance in saponin-deficient plants. *Proc. Natl Acad. Sci. USA* **96,** 12923–12928 (1999).
20. Haralampidis, K. *et al.* A new class of oxidosqualene cyclases directs synthesis of antimicrobial phytoprotectants in monocots. *Proc. Natl Acad. Sci. USA* **98,** 13431–13436 (2001).
21. Reimmann, C. & VanEtten, H. D. Cloning and characterization of the PDA6–1 gene encoding a fungal cytochrome P-450 which detoxifies the phytoalexin pisatin from garden pea. *Gene* **146,** 221–226 (1994).
22. Bouarab, K., Melton, R., Peart, J., Baulcombe, D. & Osbourn, A. A saponin-detoxifying enzyme mediates suppression of plant defences. *Nature* **418,** 889–892 (2002).
23. Sesma, A. & Osbourn, A. E. The rice leaf blast pathogen undergoes developmental processes typical of root-infecting fungi. *Nature* **431,** 582–586 (2004).
24. Murashige, T. & Skoog, F. A revised medium for rapid growth and bioassays with tobacco tissue cultures. *Physiol. Plant.* **15,** 473–497 (1962).
25. Whalen, M. C., Innes, R. W., Bent, A. F. & Staskawicz, B. J. Identification of *Pseudomonas syringae* pathogens of *Arabidopsis* and a bacterial locus determining avirulence on both *Arabidopsis* and soybean. *Plant Cell* **3,** 49–59 (1991).
26. Lindgren, P. B., Peet, R. C. & Panopoulos, N. J. Gene cluster of *Pseudomonas syringae* pv. '*phaseolicola*' controls pathogenicity of bean plants and hypersensitivity of nonhost plants. *J. Bacteriol.* **168,** 512–522 (1986).
27. Fillingham, A. J. *et al.* Avirulence genes from *Pseudomonas syringae* pathovars *phaseolicola* and *pisi* confer specificity towards both host and non-host species. *Physiol. Mol. Plant Pathol.* **40,** 1–15 (1992).
28. Rich, J. J., Hirano, S. S. & Willis, D. K. Pathovar-specific requirement for the *Pseudomonas syringae lemA* gene in disease lesion formation. *Appl. Environ. Microbiol.* **58,** 1440–1446 (1992).
29. Brooks, D. M. *et al.* Identification and characterization of a well-defined series of coronatine biosynthetic mutants of *Pseudomonas syringae* pv. *tomato* DC3000. *Mol. Plant Microbe Interact.* **17,** 162–174 (2004).
30. National Committee for Clinical Laboratory Standards (NCCLS). *Methods for Dilution Antimicrobial Susceptibility Tests for Bacteria that Grow Aerobically. Approved Standard M7–A6* 5th edn (NCCLS, Wayne, Pennsylvania, USA, 2003).


**Supplementary Information** accompanies the paper on **www.nature.com/nature**.

**Acknowledgements** We thank W. Songnuan and J. Dangl for critical reading of the manuscript, and E. Wortman-Wunder for editing suggestions. This work was supported by the Colorado State University Agricultural Experiment Station (J.M.V.) and by NIH and NSF grants to F.M.A. J.M.V. is a NSF-CAREER Faculty Fellow.

**Competing interests statement** The authors declare that they have no competing financial interests.

**Correspondence** and requests for materials should be addressed to J.M.V. (j.vivanco@colostate.edu) or F.M.A. (ausubel@molbio.mgh.harvard.edu).

# Spike-timing-dependent synaptic plasticity depends on dendritic location

**Robert C. Froemke, Mu-ming Poo & Yang Dan**

*Department of Molecular and Cell Biology and Helen Wills Neuroscience Institute, University of California, Berkeley, California 94720-3200, USA*

**In the neocortex, each neuron receives thousands of synaptic inputs distributed across an extensive dendritic tree. Although postsynaptic processing of each input is known to depend on its dendritic location[1–8], it is unclear whether activity-dependent synaptic modification is also location-dependent. Here we report that both the magnitude and the temporal specificity of spike-timing-dependent synaptic modification[9–17] vary along the apical dendrite of rat cortical layer 2/3 pyramidal neurons. At the distal dendrite, the magnitude of long-term potentiation is smaller, and the window of pre-/postsynaptic spike interval for long-term depression (LTD) is broader. The spike-timing window for LTD correlates with the window of action potential-induced suppression of NMDA (*N*-methyl-D-aspartate) receptors; this correlation applies to both their dendritic location-dependence and pharmacological properties. Presynaptic stimulation with partial blockade of NMDA receptors induced LTD and occluded further induction of spike-timing-dependent LTD, suggesting that NMDA receptor suppression underlies LTD induction. Computer simulation studies showed that the dendritic inhomogeneity of spike-timing-dependent synaptic modification leads to differential input selection at distal and proximal dendrites according to the temporal characteristics of presynaptic spike trains. Such location-dependent tuning of inputs, together with the dendritic heterogeneity of postsynaptic processing, could enhance the computational capacity of cortical pyramidal neurons.**

Whole-cell recordings were made from layer 2/3 pyramidal neurons in rat cortical slices[14]. To activate synapses selectively at each dendritic location, two extracellular stimulating electrodes were placed $<10\,\mu m$ away from the apical dendrite, one $<50\,\mu m$ from the soma ('proximal') and one $>100\,\mu m$ from the soma ('distal', Fig. 1a). Both electrodes reliably evoked excitatory postsynaptic potentials (EPSPs) from separate populations of synapses, as indicated by linear EPSP summation[3,7] (Fig. 1b) and the absence of paired-pulse depression between the inputs. To induce long-term synaptic modification, postsynaptic action potentials (APs) were paired with presynaptic stimulation of one input (60 pairs, 0.2 Hz). At the paired input, pre → post pairing (presynaptic stimulation followed by postsynaptic stimulation) induced long-term potentiation (LTP) and post → pre pairing (postsynaptic stimulation followed by presynaptic stimulation) induced long-term depression (LTD) (Fig. 1c), consistent with spike-timing-dependent plasticity (STDP) of these synapses[14]. Interestingly, there are quantitative differences in the temporal window for proximal and distal inputs (Fig. 1d). Although the magnitude of LTP was smaller distally than proximally, the main difference was in the width of the LTD window, with the distal window markedly broader than the proximal window. In particular, with a pre-/postsynaptic spike interval of $-100 < \Delta t < -50\,ms$ (Fig. 1d, dotted box), LTD was absent at proximal synapses ($-1.9 \pm 2.7\%$, $n = 8$; $P > 0.2$, *t*-test), but was still observed at distal synapses ($-22.6 \pm 3.4\%$, $n = 13$, $P < 0.00001$). This difference in the LTD window was also found with the $GABA_A$ receptor antagonist picrotoxin (10 μM) in the bath (see Supplementary Fig. 1).

Induction of LTP by pre → post pairing may depend on supralinear summation of EPSPs and back-propagating APs[9,15,18]. The

smaller magnitude of LTP at the distal dendrite may be due to attenuation of the AP[9,18–21] over the length of the dendrite. For LTD induced by post → pre pairing, however, little is known about the underlying mechanism. We therefore performed a series of experiments examining the properties of distal and proximal dendrites that may account for the difference in the LTD window. We first measured the temporal interaction between EPSPs and back-propagating APs by making dendritic recordings either distally or proximally to measure the EPSP, the antidromically-evoked AP, and the paired AP and EPSP (Fig. 2a). In contrast to supralinear summation between EPSP → AP pairs[9,15,18,21,22], we found significant suppression of EPSPs in AP → EPSP pairs. This suppression had different temporal windows for distal and proximal inputs (Fig. 2b), reminiscent of the LTD windows (Fig. 1d). Such difference in the EPSP suppression window found in dendritic recordings (see Supplementary Fig. 2) was also detected in somatic recordings (Fig. 2c), a method used routinely in subsequent experiments.

The EPSP suppression in AP → EPSP pairs might be due to a reduction in presynaptic glutamate release (for example, caused by retrograde signals[23]) or changes in postsynaptic responsiveness[6,24–26]. When glutamate pulses were applied iontophoretically at each dendritic site, we found significant suppression of the responses by the preceding AP (Fig. 2d), with temporal windows similar to those for EPSPs (Fig. 2c). This is consistent with a postsynaptic mechanism. We next examined whether the AP induces suppression of the synaptic response mediated by AMPARs (α-amino-3-hydroxy-5-methyl-4-isoxazole propionic acid receptors) or NMDA receptors (NMDARs). After isolation of AMPAR-mediated EPSPs (AMPAR-EPSPs) using the selective NMDAR antagonist AP5 (D(-)-2-amino-5-phosphonovaleric acid, 50 μM) and picrotoxin, we found that APs induced suppression of AMPAR-EPSPs, but with similar windows at distal and proximal dendrites (somatic recording, Fig. 2e; dendritic recording, Supplementary Fig. 3). This transient suppression may reflect shunting of AMPAR-EPSPs[6]. However, for NMDAR-EPSPs measured in the presence of CNQX (6-cyano-7-nitroquinoxaline-2,3-dione, 20 μM) and picrotoxin, the suppression window was significantly broader distally than proximally (somatic recording, Fig. 2f; dendritic recording, Supplementary Fig. 3), resembling the windows for EPSP suppression with AP → EPSP pairing (Fig. 2b, c). These results suggest that suppression of NMDAR-EPSPs sets the spike-timing window for LTD.

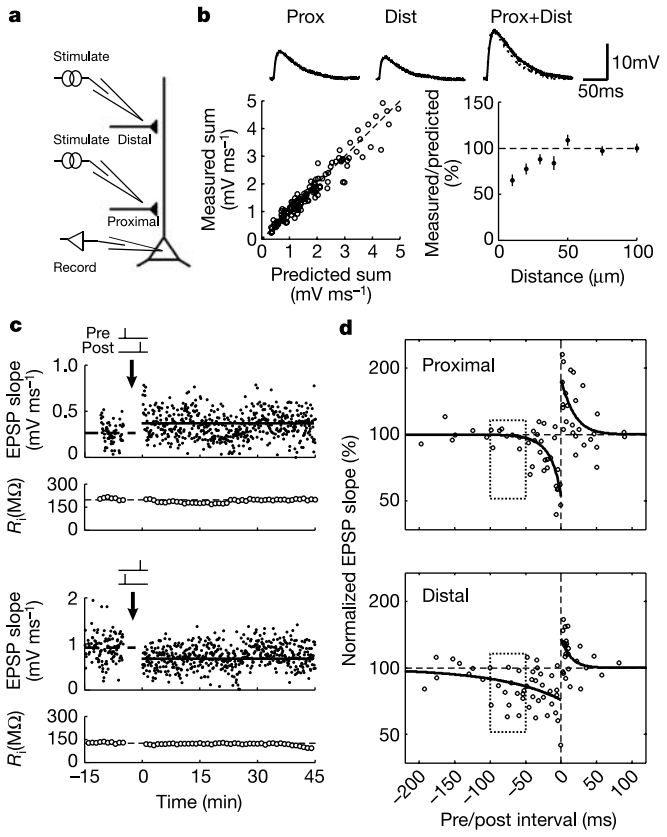


**Figure 1** Spike-timing-dependent synaptic modification at proximal and distal dendrites. **a**, Experimental configuration. **b**, Focal stimulation activates separate distal and proximal inputs. Upper panel, recorded (solid) and predicted (dotted) EPSPs. Lower left, EPSP evoked by simultaneous stimulation versus linear prediction ($n = 110$). Lower right, measured/predicted EPSP ratio (mean ± s.e.m., $n = 4$–13) versus distance between stimulation sites. **c**, Top, example of LTP (EPSP slope: 48%; peak: 68%, not shown) of distal input induced by pre → post pairing ($\Delta t = 2$ ms). Lines indicate means before (dashed) and 11–20 min after (solid) induction (arrow). Bottom, example of LTD (slope: −22%; peak: −19%) of distal input by post → pre pairing ($\Delta t = -52$ ms). **d**, Synaptic modification versus spike interval. Curves, single-exponential fits. Proximal: $A_+ = 0.76$, $\tau_+ = 15.9$ ms ($n = 26$); $A_- = -0.48$, $\tau_- = 19.3$ ms ($n = 38$). Distal: $A_+ = 0.36$, $\tau_+ = 12.5$ ms ($n = 24$); $A_- = -0.28$, $\tau_- = 103.4$ ms ($n = 46$).

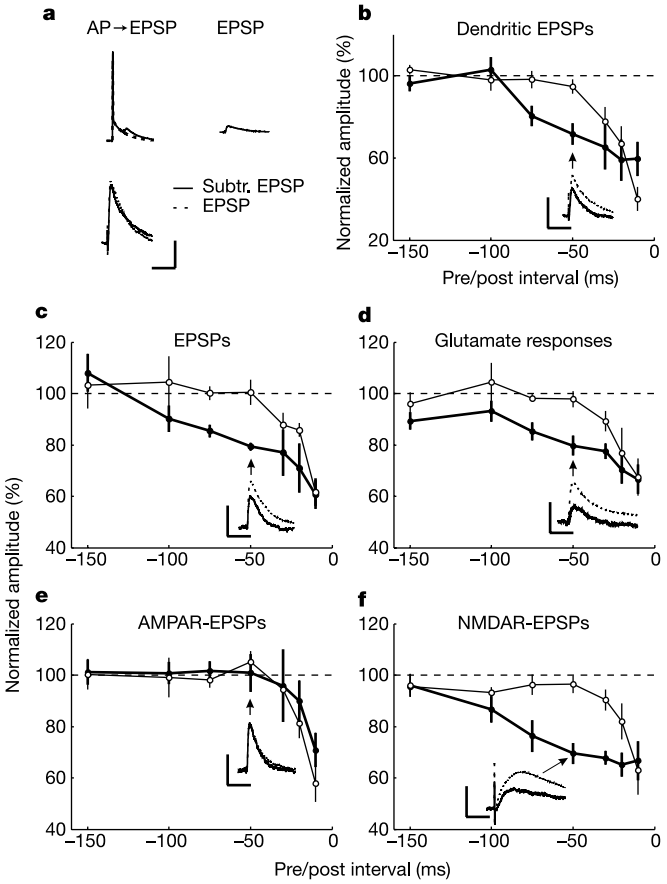


**Figure 2** Suppression of EPSP by back-propagating action potential. **a**, Top, dendritic recordings (23 μm from soma) of AP → EPSP pair (solid, $\Delta t = -46$ ms), AP (dashed), and control EPSP. Bottom, subtracted and control EPSPs; no suppression in this case. Scale: 40 mV (top), 4 mV (bottom); 100 ms. **b**, Temporal windows of AP → EPSP suppression in distal (filled circles) and proximal (open circles) dendrites. Subtracted EPSP amplitude normalized by control (mean ± s.e.m., $n = 4$–9) versus pre/post interval. Inset: subtracted ($\Delta t = -49$ ms) and control EPSPs recorded from distal dendrite (110 μm). Scale: 2 mV; 100 ms. **c**–**f**, Similar to (**b**) except that recordings were made somatically. Distal inputs (filled circles); proximal inputs (open circles). AP-induced suppression of EPSPs (**c**), responses to glutamate pulses (**d**), AMPAR-EPSPs (**e**), and NMDAR-EPSPs (**f**) versus pre/post interval. $n = 4$–12. Scale: 4 mV (**c**) and 2 mV (**d**–**f**); 100 ms.

Dendritic recordings showed that suppression occurred in the absence of after-hyperpolarization (Fig. 2a and Supplementary Fig. 2a), indicating that it is unlikely to be caused by hyperpolarization-induced increase in $Mg^{2+}$ block of NMDARs. Another possible mechanism is NMDAR desensitization[24–26], perhaps triggered by $Ca^{2+}$ influx through AP-activated channels. To test this possibility, we measured AP-induced suppression of NMDAR-EPSPs after postsynaptic loading of BAPTA (5 mM), a high-affinity $Ca^{2+}$ chelator, through the whole-cell pipette. As shown in Fig. 3a, BAPTA blocked the NMDAR-EPSP suppression, indicating that the suppression is $Ca^{2+}$-dependent. The suppression is also largely abolished by bath application of the L-type calcium channel antagonist nimodipine (10 μM, Fig. 3b), indicating that $Ca^{2+}$ influx through L-type channels is required. Finally, postsynaptic loading of calcineurin inhibitory peptide (CIP, 270 μM, Fig. 3c) or infection of the cell with a viral vector expressing a peptide corresponding to the calcineurin-interacting domain of the NR2A subunit of NMDARs (see Supplementary Fig. 4a) largely abolished AP-induced NMDAR-EPSP suppression, indicating that calcineurin is required. Together, these results strongly suggest that AP-induced NMDAR-EPSP suppression is related to $Ca^{2+}$-dependent NMDAR desensitization[24–26].

To examine the relationship between NMDAR-EPSP suppression and LTD, we performed pharmacological experiments on LTD induction. We found that LTD induction by post → pre pairing depends on NMDARs[13,17], as it was blocked by AP5 (Fig. 3d). More importantly, LTD was abolished by BAPTA, CIP, nimodipine[13,17] (Fig. 3d), or viral expression of the NR2A peptide (see Supplementary Fig. 4b). We also measured dendritic $Ca^{2+}$ elevation triggered by somatically elicited single APs using two-photon imaging, and found that $Ca^{2+}$ signals were larger distally (101 ± 17 μm; ±s.d.) than proximally (21 ± 6 μm) (see Supplementary Fig. 5a, b), consistent with previous reports[20,21]. These larger $Ca^{2+}$ signals may cause longer suppression of NMDAR-EPSPs and thereby widen the LTD window. To examine further the relationship between AP-evoked dendritic $Ca^{2+}$ signals and the windows for EPSP suppression and LTD induction, we bath-applied the $K^+$ channel blocker 4-aminopyridine (3 mM) to broaden the AP[15,17] (see Supplementary Fig. 2c). We found that 4-aminopyridine caused a significant but reversible increase in AP-induced $Ca^{2+}$ signals proximally (see Supplementary Fig. 5c). Importantly, 4-aminopyridine (in the recording pipette) also caused significant broadening of the proximal windows for NMDAR-EPSP suppression and LTD (Fig. 3e, f). Thus, the suppression and LTD windows co-vary with AP-induced dendritic $Ca^{2+}$ signals, supporting the hypothesis that $Ca^{2+}$-dependent suppression of NMDAR-EPSPs

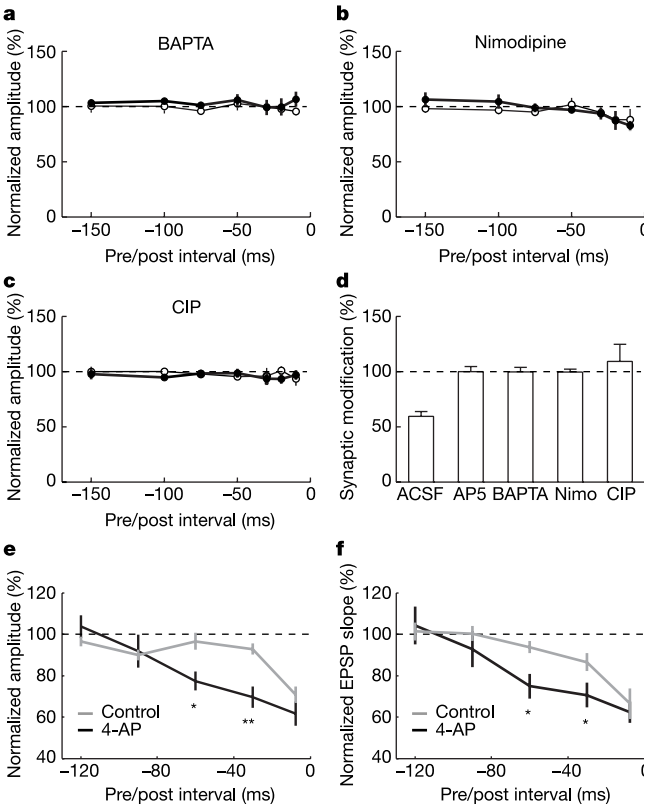


**Figure 3** Pharmacological properties of NMDAR-EPSP suppression and LTD. **a**–**c**, AP-induced NMDAR-EPSP suppression for distal (filled circles) and proximal (open circles) inputs with BAPTA (**a**), nimodipine (**b**) or CIP (**c**); $n = 4$–6. **d**, LTD induced by post → pre pairing ($\Delta t$: −6.4 ± 3.3 ms, s.d.) in normal ACSF and in presence of pharmacological agents ($n = 5$–18). Error bars show s.e.m. **e**, Temporal windows of AP-induced suppression of NMDAR-EPSPs at proximal dendrite with or without 4-aminopyridine (4-AP) ($n = 4$–8). Single asterisk, $P < 0.05$; double asterisk, $P < 0.01$; *t*-test. **f**, Temporal windows for LTD of proximal inputs induced by post → pre pairing with or without 4-aminopyridine ($n = 2$–13).

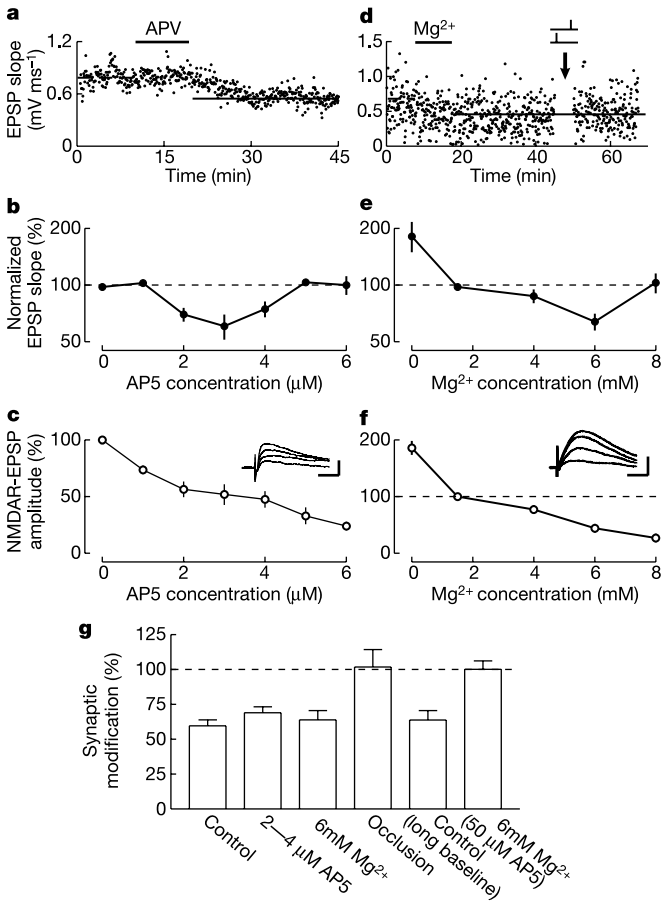


**Figure 4** Synaptic modification induced by presynaptic stimulation under partial NMDAR blockade. **a**, Example LTD (−28.8%) induced by 2 μM AP5. Black bar shows AP5 wash-in (10 min for all experiments). **b**, LTD versus AP5 concentration. Error bars show s.e.m. ($n = 3$–5). **c**, NMDAR-EPSP versus AP5 concentration ($n = 4$). Inset, NMDAR-EPSPs (0, 1, 3, 5 μM AP5). Scale: 0.5 mV; 35 ms. **d**–**f**, Similar to **a**–**c**, except with $Mg^{2+}$ washed in. **d**, LTD following 6 mM $Mg^{2+}$ wash-in: −32.4%. Post → pre pairing was applied 20 min after washout. **e**, $n = 3$–5. **f**, $n = 4$–7. Inset, NMDAR-EPSPs (1.5, 4, 6, 8 mM $[Mg^{2+}]_o$). Scale: 1 mV; 50 ms. **g**, Summary of LTD induced by AP5 and $Mg^{2+}$. Control: post → pre pairing; occlusion: post → pre pairing 20–30 min after washout of 6 mM $[Mg^{2+}]_o$; control (long baseline): post → pre pairing after 25–45 min of recording. Error bars show s.e.m. ($n = 3$–18).

determines the spike-timing window for LTD. A recent study in layer 5 of the visual cortex indicated that endocannabinoids serve as retrograde messengers for spike-timing-dependent LTD, and blocking their degradation widened the LTD window[16]. We note that, in addition to the potential existence of layer-specific mechanisms, the previous and current studies addressed different loci in the cellular pathways leading to LTD.

To determine whether reduction of NMDAR activation is sufficient for LTD, we partially blocked NMDARs using bath application of AP5 or by altering the bath concentration of $Mg^{2+}$ ($[Mg^{2+}]_o$), instead of using postsynaptic APs. We found that presynaptic stimulation alone (0.2 Hz) induced long-lasting synaptic depression with low concentrations of AP5 (2–4 μM, $P < 0.05$), but not in the absence of or at high concentrations of AP5 (Fig. 4a–c, g). Similarly, presynaptic stimulation induced significant depression with 6 mM $[Mg^{2+}]_o$ ($P < 0.01$), but not with ≤4 or 8 mM $[Mg^{2+}]_o$ (Fig. 4d–g). Importantly, post → pre pairing induced LTD after 25–45 min of baseline recording, but post → pre pairing following 6 mM $[Mg^{2+}]_o$-induced depression failed to induce LTD (Fig. 4d, g). Therefore, $Mg^{2+}$-induced depression occluded pairing-induced LTD, suggesting common mechanisms for both processes. Furthermore, we found that $Mg^{2+}$-induced synaptic depression is NMDAR-dependent, as it is abolished by AP5 (Fig. 4g). Together, these results indicate that partial block of NMDARs is sufficient to induce LTD. Since the primary role of NMDAR activation in LTP/LTD induction is to control $Ca^{2+}$ influx[13,27], our results support the hypothesis that AP-induced reduction of NMDAR-mediated $Ca^{2+}$ entry (which may depend on cell type[22,28]) leads to LTD, which fits well with the conventional model that links changes in intracellular $Ca^{2+}$ with LTD induction[13,17,27]. Interestingly, in 0 mM $[Mg^{2+}]_o$, which boosted NMDAR-EPSPs (Fig. 4f), presynaptic stimulation alone produced long-lasting EPSP enhancement (Fig. 4e, $P < 0.05$), consistent with the notion that enhanced $Ca^{2+}$ influx through NMDARs induces LTP[9,13,17,27].

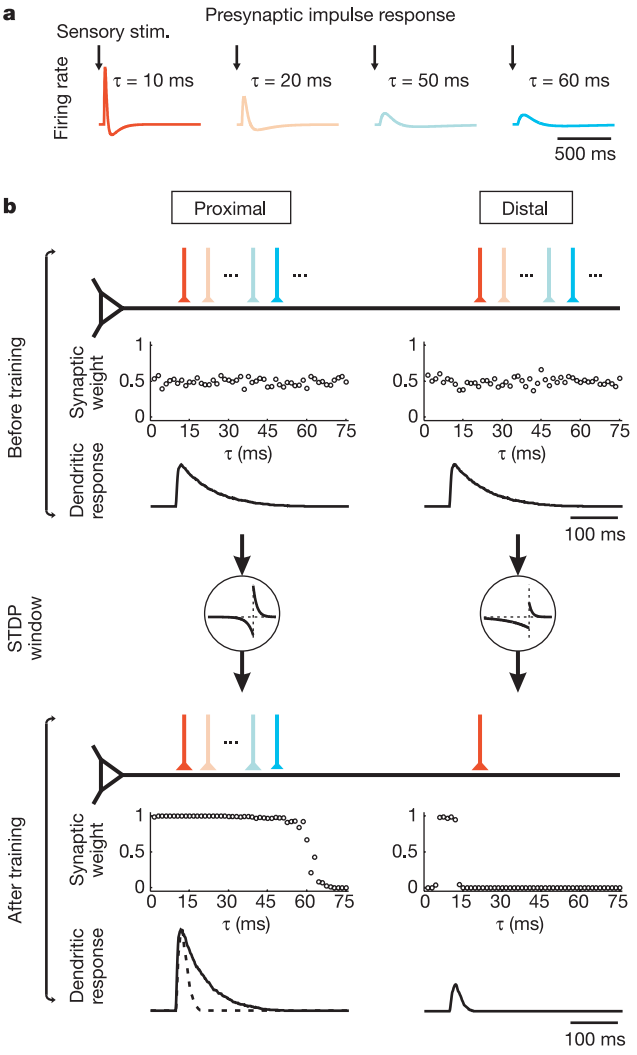


**Figure 5** Simulation of location-dependent selection of synaptic inputs. **a**, Example presynaptic responses to brief sensory stimulus. Warmer colours, more transient responses. **b**, Synaptic inputs before and after 30 min of sensory stimuli. Shown are diagrams of input patterns, synaptic weights versus $\tau$, and dendritic responses to brief sensory stimulus (see Supplementary Methods, equation (2)). To facilitate comparison of response time course after training, the distal dendritic response was scaled up (dashed line) to match the peak amplitude of the proximal response.

What are the functional consequences of the dendritic inhomogeneity in spike-timing-dependent synaptic modification? Previous theoretical studies show that LTD induced by post → pre pairing preferentially weakens inputs with long response latencies[29]. The different LTD windows reported here (Fig. 1d) may lead to differential input selectivity along the apical dendrite. To test this idea, we constructed a simple model (see Methods) in which the proximal and distal dendrites of the postsynaptic neuron exhibit different STDP windows, based on our experimental data. This neuron receives multiple inputs driven by the same sensory stimuli, but with different temporal response characteristics (Fig. 5a). Starting with similar connection strengths for all inputs, we simulated presynaptic spike trains driven by random stimuli, then simulated the postsynaptic spike train by integrating all synaptic inputs and modified each connection according to the STDP windows. We found that transient inputs were strengthened and sustained inputs were weakened both distally and proximally, but the distal dendrite was much more selective (Fig. 5b). Comparison of the dendritic responses to a brief sensory stimulus showed that, although initially similar, the response became much more transient at distal than at proximal dendrites after training. Thus, the different STDP windows may lead to functional differentiation of the distal and proximal dendrites in receiving signals with distinct temporal characteristics. Owing to the selection for transient inputs, distal dendrites may be specialized for processing the precise timing of sensory signals.

Spike-timing-dependent plasticity is a robust learning rule in the central nervous system[9–17]. Although the basic asymmetry in the spike-timing window is found at many synapses, the width of the window, especially that for LTD induction, can be highly variable[11]. Our findings indicate that such variability may be attributed in part to differences in the dendritic location of the synapses and in the temporal dynamics of AP-induced $Ca^{2+}$ elevation that leads to NMDAR desensitization. More importantly, the location-specific STDP windows provide a mechanism for developmental segregation of inputs carrying different sensory signals. Although spatial inhomogeneity in the electrical properties and nonlinearity in dendritic integration endow individual pyramidal neurons with enhanced processing capacity[5,8], the computational power can only be harvested if inputs carrying different signals are parsed into distinct dendritic regions[8,30]. The present findings not only demonstrate dendritic inhomogeneity in activity-dependent synaptic modification, but also point to its potential role in the formation of location-specific synaptic inputs, a feature that could greatly enrich the repertoire of dendritic information processing. □

## Methods

### Visual cortical slice preparation

Acute visual cortical slices were prepared from 2–4-week-old Sprague–Dawley rats. Rats were deeply anaesthetized with halothane, decapitated, and the brain quickly placed into ice-cold dissection buffer containing 206 mM sucrose, 2.5 mM KCl, 2 mM $MgSO_4$,

1.25 mM $NaH_2PO_4$, 1 mM $CaCl_2$, 1 mM $MgCl_2$, 26 mM $NaHCO_3$ and 10 mM dextrose, bubbled with 95% $O_2$/5% $CO_2$ (pH 7.4). Slices (300–400 $\mu$m thick) were prepared with a vibratome (Pelco), placed in warm dissection buffer (33–35 °C) for <30 min, transferred to a holding chamber containing artificial cerebrospinal fluid (ACSF: 124 mM NaCl, 2 mM KCl, 1.5 mM $MgSO_4$, 1.25 mM $NaH_2PO_4$, 2.5 mM $CaCl_2$, 26 mM $NaHCO_3$, 10 mM dextrose), and kept at 22–24°C for >1 h before use. For experiments, slices were transferred to the recording chamber and perfused (4.0–4.5 ml $min^{-1}$) with oxygenated ACSF at 22–24 °C.

### Electrophysiology

Somatic and dendritic whole-cell recordings were made in current-clamp with an Axopatch 200B amplifier (Axon) using infrared differential interference optics (IR-DIC) video microscopy. Layer 2/3 pyramidal cells were selected based on morphological and electrophysiological criteria[12,14]. Patch pipettes (somatic: 3–8 MΩ; dendritic: 8–20 MΩ) were filled with intracellular solution (120 mM K-gluconate, 10 mM HEPES, 0.1 mM EGTA, 20 mM KCl, 2 mM $MgCl_2$, 10 mM phosphocreatine, 2 mM ATP, and 0.25 mM GTP). The mean resting potential was $-70.3 \pm 0.7$ mV, corrected for the measured liquid junction potential (6.8 mV). The series resistance was $14.6 \pm 1.6$ MΩ. Input resistance ($R_i = 118.0 \pm 5.4$ MΩ) was monitored with hyperpolarizing current pulses (50 pA, 100 ms); cells were excluded if $R_i$ changed >30% over the entire experiment[12,14]. Data were filtered at 2 kHz, digitized at 10 kHz and analysed with Clampfit 8 (Axon). EPSPs were evoked by focal extracellular stimulation (0.01–1 ms, 1–100 V) with small glass bipolar electrodes. To ensure that the distal (>100 $\mu$m from soma) and proximal (<50 $\mu$m) electrodes activated separate synapses, we tested both the linear summation of EPSPs (Fig. 1b) and paired-pulse depression between inputs. Although consecutive stimulation through the same electrode induced marked paired-pulse depression of these synapses, no depression was induced by sequential stimulation through the two electrodes, indicating that they activated separate synapses. Postsynaptic APs were elicited either with depolarizing current injection through the recording electrode (1 nA, 1–4 ms; somatic recordings) or antidromically with an extracellular stimulating electrode near the axonal initial segment (0.01–1 ms, 5–100 V; dendritic recordings). Presynaptic spike timing was defined as the onset of EPSP and postsynaptic spike timing was measured at the AP peak[12,14]. Synaptic strength was measured as the initial slope (first 2 ms) of the EPSP. To measure long-term synaptic modification, a stable baseline of synaptic strength was first established by 6–12 min of recording with presynaptic stimulation at 0.2 Hz. Synaptic strength after induction was measured 11–20 min after the end of induction. For iontophoretic application of glutamate, a sharp microelectrode (150–200 MΩ) filled with 250 mM $Na^+$-glutamate was positioned near the apical dendrite (<5 $\mu$m). Both the holding current (1–10 nA) and ejection current (100–300 nA, 0.01–3 ms) were applied with an amplifier (Getting)[3].

### Model simulation

The model consisted of one postsynaptic neuron and 100 presynaptic inputs (50 to the proximal and 50 to the distal dendrite, see diagram in Fig. 5b). The presynaptic neurons had a range of response time courses (Fig. 5a) but they were all driven by the same sensory stimulus, which was a temporally varying random signal (see Supplementary Fig. 6a). The spike train of the postsynaptic cell was simulated after integrating the synaptic input to both the distal and proximal dendritic compartments. All connection weights were initialized to 0.5 plus a small random number (Fig. 5b, upper panel), and were modified according to the STDP windows measured experimentally. Details of the model are given in Supplementary Methods.

Received 11 May; accepted 23 December 2004; doi:10.1038/nature03366.


1. Stuart, G. & Spruston, N. Determinants of voltage attenuation in neocortical pyramidal neuron dendrites. *J. Neurosci.* **18,** 3501–3510 (1998).
2. Larkum, M. E., Zhu, J. J. & Sakmann, B. A new cellular mechanism for coupling inputs arriving at different cortical layers. *Nature* **398,** 338–341 (1999).
3. Cash, S. & Yuste, R. Linear summation of excitatory inputs by CA1 pyramidal neurons. *Neuron* **22,** 383–394 (1999).
4. Magee, J. C. Dendritic integration of excitatory synaptic input. *Nature Rev. Neurosci.* **1,** 181–190 (2000).
5. Segev, I. & London, M. Untangling dendrites with quantitative models. *Science* **290,** 744–750 (2000).
6. Hausser, M., Major, G. & Stuart, G. J. Differential shunting of EPSPs by action potentials. *Science* **291,** 138–141 (2001).
7. Tamas, G., Szabadics, J. & Somogyi, P. Cell type- and subcellular position-dependent summation of unitary postsynaptic potentials in neocortical neurons. *J. Neurosci.* **22,** 740–747 (2002).
8. Hausser, M. & Mel, B. Dendrites: bug or feature? *Curr. Opin. Neurobiol.* **13,** 372–383 (2003).
9. Magee, J. C. & Johnston, D. A. synaptically controlled, associative signal for Hebbian plasticity in hippocampal neurons. *Science* **275,** 209–213 (1997).
10. Markram, H., Lubke, J., Frotscher, M. & Sakmann, B. Regulation of synaptic efficacy by coincidence of postsynaptic APs and EPSPs. *Science* **275,** 213–215 (1997).
11. Sourdet, V. & Debanne, D. The role of dendritic filtering in associative long-term synaptic plasticity. *Learn. Mem.* **6,** 422–447 (1999).
12. Feldman, D. E. Timing-based LTP and LTD at vertical inputs to layer II/III pyramidal cells in rat barrel cortex. *Neuron* **27,** 45–56 (2000).
13. Bi, G. & Poo, M. Synaptic modification by correlated activity: Hebb's postulate revisited. *Annu. Rev. Neurosci.* **24,** 139–166 (2001).
14. Froemke, R. C. & Dan, Y. Spike-timing-dependent synaptic modification induced by natural spike trains. *Nature* **416,** 433–438 (2002).
15. Watanabe, S., Hoffman, D. A., Migliore, M. & Johnston, D. Dendritic K+ channels contribute to spike-timing dependent long-term potentiation in hippocampal pyramidal neurons. *Proc. Natl Acad. Sci. USA* **99,** 8366–8371 (2002).
16. Sjostrom, P. J., Turrigiano, G. G. & Nelson, S. B. Neocortical LTD via coincident activation of presynaptic NMDA and cannabinoid receptors. *Neuron* **39,** 641–654 (2003).
17. Johnston, D. *et al.* Active dendrites, potassium channels and synaptic plasticity. *Phil. Trans. R. Soc. Lond. B Biol. Sci.* **358,** 667–674 (2003).
18. Stuart, G. J. & Hausser, M. Dendritic coincidence detection of EPSPs and action potentials. *Nature Neurosci.* **4,** 63–71 (2001).
19. Golding, N. L., Staff, N. P. & Spruston, N. Dendritic spikes as a mechanism for cooperative long-term potentiation. *Nature* **418,** 326–331 (2002).
20. Svoboda, K., Helmchen, F., Denk, W. & Tank, D. W. Spread of dendritic excitation in layer 2/3 pyramidal neurons in rat barrel cortex *in vivo*. *Nature Neurosci.* **2,** 65–73 (1999).
21. Waters, J., Larkum, M., Sakmann, B. & Helmchen, F. Supralinear $Ca^{2+}$ influx into dendritic tufts of layer 2/3 neocortical pyramidal neurons *in vitro* and *in vivo*. *J. Neurosci.* **22,** 8558–8567 (2003).
22. Koester, H. J. & Sakmann, B. Calcium dynamics in single spines during coincident pre- and postsynaptic activity depend on relative timing of back-propagating action potentials and subthreshold excitatory postsynaptic potentials. *Proc. Natl Acad. Sci. USA* **95,** 9596–9601 (1998).
23. Zilberter, Y., Kaiser, K. M. & Sakmann, B. Dendritic GABA release depresses excitatory transmission between layer 2/3 pyramidal and bitufted neurons in rat neocortex. *Neuron* **24,** 979–988 (1999).
24. Rosenmund, C., Feltz, A. & Westbrook, G. L. Calcium-dependent inactivation of synaptic NMDA receptors in hippocampal neurons. *J. Neurophysiol.* **73,** 427–430 (1995).
25. Tong, G., Shepherd, D. & Jahr, C. E. Synaptic desensitization of NMDA receptors by calcineurin. *Science* **267,** 1510–1512 (1995).
26. Umemiya, M., Chen, N., Raymond, L. A. & Murphy, T. H. A calcium-dependent feedback mechanism participates in shaping single NMDA miniature EPSCs. *J. Neurosci.* **21,** 1–9 (2001).
27. Zucker, R. S. Calcium- and activity-dependent synaptic plasticity. *Curr. Opin. Neurobiol.* **9,** 305–313 (1999).
28. Nevian, T. & Sakmann, B. Single spine $Ca^{2+}$ signals evoked by coincident EPSPs and backpropagating action potentials in spiny stellate cells of layer 4 in the juvenile rat somatosensory barrel cortex. *J. Neurosci.* **24,** 1689–1699 (2004).
29. Song, S., Miller, K. D. & Abbott, L. F. Competitive Hebbian learning through spike-timing-dependent synaptic plasticity. *Nature Neurosci.* **3,** 919–926 (2000).
30. Archie, K. A. & Mel, B. W. A model for intradendritic computation of binocular disparity. *Nature Neurosci.* **3,** 54–63 (2000).


**Supplementary Information** accompanies the paper on **www.nature.com/nature**.

**Acknowledgements** We thank P. Ascher, G. Bi, L. Chen, M. Frerking, E. Isacoff, R. Kramer and R. Zucker for helpful discussions, and K. Arendt, K. Borges, N. Caporale and C. Nam for technical assistance. This work was supported by grants from the National Eye Institute and the Grass Foundation. R.C.F. is a recipient of the Howard Hughes Predoctoral Fellowship.

**Competing interests statement** The authors declare that they have no competing financial interests.

**Correspondence** and requests for materials should be addressed to Y.D. (ydan@berkeley.edu).

# The receptors and coding logic for bitter taste

**Ken L. Mueller[1], Mark A. Hoon[2], Isolde Erlenbach[2], Jayaram Chandrashekar[1], Charles S. Zuker[1] & Nicholas J. P. Ryba[2]**

[1]*Howard Hughes Medical Institute and Departments of Biology and Neurosciences, University of California at San Diego, La Jolla, California 92093-0649, USA*
[2]*National Institute of Dental and Craniofacial Research, National Institutes of Health, Bethesda, Maryland 20892, USA*

**The sense of taste provides animals with valuable information about the nature and quality of food. Bitter taste detection functions as an important sensory input to warn against the ingestion of toxic and noxious substances. T2Rs are a family of approximately 30 highly divergent G-protein-coupled receptors (GPCRs)[1,2] that are selectively expressed in the tongue and palate epithelium[1] and are implicated in bitter taste sensing[1–8]. Here we demonstrate, using a combination of genetic, behavioural and physiological studies, that T2R receptors are necessary and sufficient for the detection and perception of bitter compounds, and show that differences in T2Rs between species (human and mouse) can determine the selectivity of bitter taste responses. In addition, we show that mice engineered to express a bitter taste**